Progress In Electromagnetics Research, Vol. 124, 473–486, 2012

IMPROVEMENT OF ITERATIVE PHYSICAL OPTICS USING PREVIOUS INFORMATION TO GUIDE INITIAL GUESS

H. Chin, J.-H. Yeom, H.-T. Kim, and K.-T. Kim*

Department of Electrical Engineering, Pohang University of Science and Technology (POSTECH) San 31, Hyoja-dong, Namgu, Pohang, Gyeongbuk 790-784, Korea

Abstract—We propose an improved method of iterative physical optics (IPO) to analyze electromagnetic scattering by open-ended cavities. The traditional IPO method uses a fixed number of iterations; if this number is too small, the accuracy of the estimated monostatic radar cross section (RCS) of open-ended cavities degrades as the incident angle of the incident field increases. The recently-introduced adaptive iterative physical optics-change rate (AIPO-CR) method uses a variable number of iterations; compared to the IPO method, it predicts monostatic RCS more accurately, but requires more computation time. In this paper, a new algorithm is devised to improve both the monostatic RCS prediction accuracy of the IPO method, and the computational efficiency of the AIPO-CR method. The proposed method, iterative physical optics-retained previous solution (IPO-RPS), calculates the currents at one incident angle, then reuses them as the initial currents of iterations for the next incident angle. In simulations of the monostatic RCS for various open-ended cavities, the IPO-RPS method was more accurate than the traditional IPO method, and computationally more efficient than both the IPO and AIPO-CR methods.

1. INTRODUCTION

The radar cross section (RCS) is a fictitious area of a target from the viewpoint of the radar and generally proportional to the target's size, but an open-ended cavity usually has an RCS greater than its size. Therefore, analysis of an open-ended cavity structure has significant

Received 11 January 2012, Accepted 3 February 2012, Scheduled 8 February 2012
* Corresponding author: Kyung-Tae Kim (kkt@postech.ac.kr).

applications. For example, it is a prerequisite to design a combat plane having low RCS values.

Numerical techniques developed to analyze an open-ended cavity include low-frequency methods, such as the method of moments (MoM) [1, 2], finite element method (FEM) [3, 4], and finite different time domain (FDTD) [5–7], and high-frequency methods, such as geometrical optics (GO) [8, 9], geometrical theory of diffraction (GTD) [10], physical optics (PO) [11, 12], and the physical theory of diffraction (PTD) [13, 14]. Low-frequency methods solve Maxwell's equations with no implicit approximations and are typically limited to objects of small electrical size due to limitations of computation time and system memory. High-frequency methods invoke many approximations to make the equations of scattering problems tractable; therefore, these methods have an advantage over low-frequency methods when calculating RCS of objects that are electrically large [15]. Among them, shooting and bouncing rays (SBR) has been introduced [16–18] to account for multiple reflections in a partially-open cavity. An open-ended cavity can be analyzed efficiently using SBR, but it has a fundamental error because it is based on the rays at far fields [8]. Iterative physical optics (IPO) [19–21] also has been developed to analyze the scattering by the cavities with many multiple reflections. The IPO method calculates the unknown currents using the magnetic field integral equation (MFIE). The equation is solved iteratively starting with the initial current value, i.e., PO current. The number N of iterations required for convergence is fixed and is proportional to the expected number of important reflections [19]. The adaptive iterative physical optics-change rate (AIPO-CR) [22, 23] method does not set N in advance but determines it adaptively by analyzing the change rate (CR) of the current energy of all facets. The AIPO-CR method improves the accuracy of the solution but it has the disadvantage that the calculation time increases with the incident angle θ, because the number of multiple reflections in the cavity increases.

The method proposed in this paper, iterative physical optics-retained previous solution (IPO-RPS), improves both IPO and AIPO-CR methods by using a new initial guess based on the assumption that the value of the current does not vary greatly with θ in smooth structures [24]. Therefore, the value of the current calculated in the previous incident angle can be reused as the initial current for iterations in the subsequent incident angle. When calculating the monostatic RCS of various cavities, the proposed method is faster than both the IPO and AIPO-CR methods. The proposed method is also applicable even for rough structures by adaptive use of the new initial guess and the traditional one, i.e., PO current.

The remainder of this paper is organized as follows. Section 2 presents the numerical methods considered here to involve IPO, AIPO-CR, and IPO-RPS. Section 3 describes simulation results to show improved accuracy compared to the IPO method and enhanced efficiency compared to both the IPO and AIPO-CR methods. Section 4 contains conclusions.

2. NUMERICAL METHODS

2.1. IPO

A formulation based on the high frequency asymptotic principles of PO was developed to analyze the scattering by arbitrary open-ended cavities [19]. First, it obtains equivalent currents induced in the aperture by the incident field, and then calculates the magnetic field on the cavity using the equivalent currents. From information about the magnetic field, the currents on the interior cavity walls are obtained iteratively using the MFIE [19]:

$$\begin{aligned} \bar{J}^n_{\theta_m}(\bar{r}_c) &= 2\hat{n}\times\bar{H}(\bar{r}_c) - 2\hat{n}\times\oint_{s_c}\bar{J}^{n-1}_{\theta_m}\left(\bar{r}'_c\right)\times\nabla G_0\left(\bar{r}_c-\bar{r}'_c\right)dS'_c, \\ m &= 1,2,\ldots,M, \qquad n=1,2,\ldots,N, \end{aligned} \tag{1}$$

$$\nabla G_0(\bar{R}) = -\hat{R}\left(jk+\frac{1}{R}\right)\frac{e^{-jkR}}{4\pi R}, \tag{2}$$

where n is the iteration number, N the fixed maximum number of iterations, m is the index of incident angle, M the maximum number of incident angles considered, $\bar{J}^n_{\theta_m}(\bar{r}_c)$ and $\bar{H}(\bar{r}_c)$ the surface current and the magnetic field on the facet that includes $\bar{r}_c$, respectively, $\hat{n}$ the unit normal vector of the facet, $G_0(\bar{R})$ the Green function in free space, k the wavenumber, and time dependence $e^{j\omega t}$ assumed. In Eq. (1), the initial current value $\bar{J}^0_{\theta_m}(\bar{r}_c)$ on the right-hand side to calculate the first currents $\bar{J}^1_{\theta_m}(\bar{r}_c)$ on the left-hand side is [19].

$$\bar{J}^0_{\theta_m}(\bar{r}_c) = \begin{cases} 2\hat{n}\times\bar{H}(\bar{r}_c): & \text{lit region} \\ 0: & \text{shadow region} \end{cases}. \tag{3}$$

In the IPO method, N is chosen in advance by roughly estimating of the number of important internal reflections for the incident angle region of interests, and the PO current in Eq. (3) is used as the initial current $\bar{J}^0_{\theta_m}(\bar{r}_c)$ of iterations in Eq. (1) for each θ_m. Because N is fixed, it does not change as θ_m of the incident field increases.

2.2. AIPO-CR

The recently-introduced AIPO-CR method improves the accuracy of the IPO method by using a variable number of iterations. The number $N(m)$ of iterations for each θ_m is determined if CR(n) between the $(n-1)$th current energy sum $E(\bar{J}_{\theta_m}^{n-1})$ and the nth current energy sum $E(\bar{J}_{\theta_m}^{n})$ of all facets is less than a predetermined threshold value. $N(m)$ in the AIPO-CR method changes with θ_m of the incident field. CR(n) is given by [22]:

$$E(\bar{J}_{\theta_m}^{n}) \equiv \sum_{i}^{\text{all facets}} \sqrt{\left[\left|J_x^n(i)\right|^2\right] + \left[\left|J_y^n(i)\right|^2\right] + \left[\left|J_z^n(i)\right|^2\right]}, \quad (4)$$

$$\mathrm{CR}(n) \equiv \left|\frac{E\left(\bar{J}_{\theta_m}^{n}\right) - E\left(\bar{J}_{\theta_m}^{n-1}\right)}{E\left(\bar{J}_{\theta_m}^{n-1}\right)}\right| \times 100(\%), \quad (5)$$

where i is the index of the facet, $J_d^n(i)$ the nth surface current in the d-direction on the ith facet (d: x, y, z), and CR(n) the nth change rate. $\bar{J}_{\theta_m}^{n}$ matches the solution if $3\% \leq \mathrm{CR}(n) \leq 5\%$ [22, 23]. The AIPO-CR method improves the accuracy of the IPO solution as θ_m increases, because the method uses an adaptive number of iterations $N(m)$ for convergence, rather than the fixed N used in IPO. However, this method has a demerit that $N(m)$ (e.g., computation time) increases with θ_m.

2.3. IPO-RPS

The IPO-RPS method (Fig. 1) determines $N(m)$ in the same way as does the AIPO-CR method, but improves the estimation efficiency by using a new initial estimate that is based on information calculated at previous incident angle θ_{m-1}. As in AIPO-CR, convergence is assumed if $3\% \leq \mathrm{CR}' \leq 5\%$ [22, 23]. The criterion that the solution does not converge resulting from the poor initial value can be determined by the difference between $N(m\text{-}1)$ and n. The difference α can be any integer larger than 1, because the number of iterations required inside the cavity increases with θ.

If the magnitude of excitation source is slightly changed (for example, due to a slight change of θ_m), N can be reduced by reusing the previous solution as the initial guess [1, 24]. This process is based upon the assumption that the structure is smooth. If the structure is smooth, the induced current on the structure does not vary greatly with θ_m. Therefore, the current $\bar{J}_{\theta_{m-1}}^{N(m-1)}(\bar{r}_c)$ calculated at the previous incident angle θ_{m-1} can be reused as the initial current $\bar{J}_{\theta_m}^{0}(\bar{r}_c)$ for the

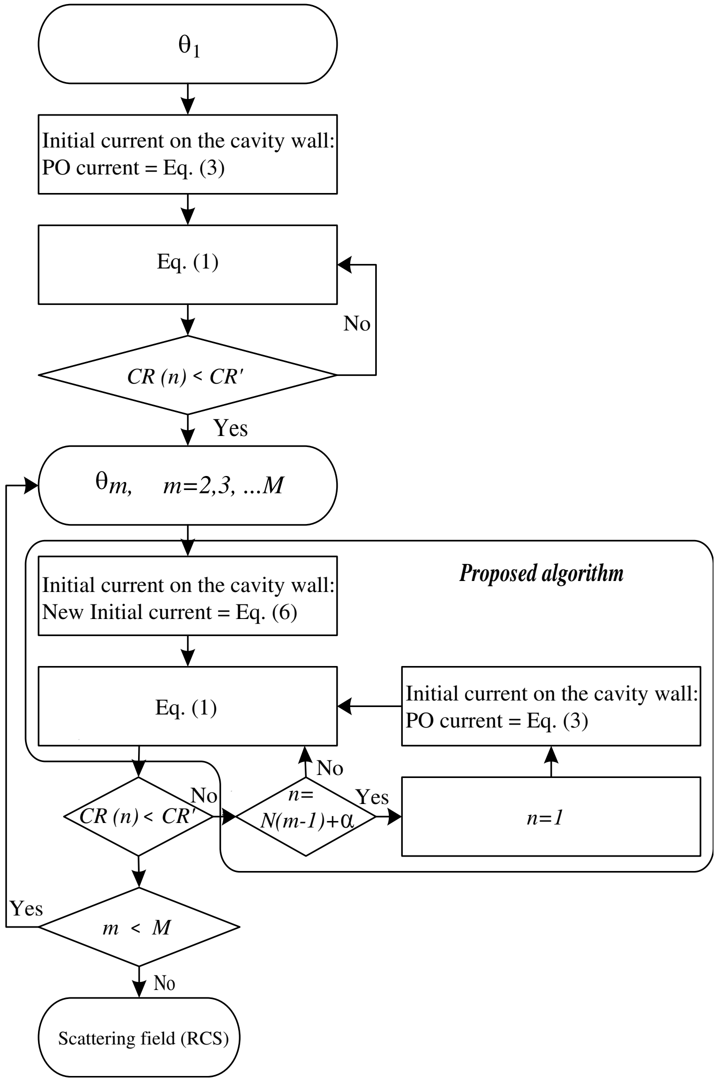

Figure 1. Flow chart of the IPO-RPS method. CR' and α are predetermined threshold values.

present incident angle θ_m. Hence, the initial value in Eq. (3) can be replaced with a new initial estimate:

$$\bar{J}^0_{\theta_m}(\bar{r}_c) = \bar{J}^{N(m-1)}_{\theta_{m-1}}(\bar{r}_c); \tag{6}$$

i.e., the $N(m-1)$th final solution for θ_{m-1} is used as the initial value for θ_m. Substituting Eq. (6) into Eq. (1) yields

$$\bar{J}^n_{\theta_m}(\bar{r}_c) = 2\hat{n} \times \bar{H}(\bar{r}_c) - 2\hat{n}\times \oint_{s_c} \bar{J}\left(\bar{r}'_c\right) \times \nabla G_0\left(\bar{r}_c - \bar{r}'_c\right) - dS'_c,$$
$$m = 1, 2, \ldots, M, \qquad n = 1, 2, \ldots, N(m), \tag{7a}$$

where

$$\bar{J}\left(\bar{r}'_c\right) = \bar{J}^{N(m-1)}_{\theta_{m-1}}\left(\bar{r}'_c\right) \quad m \geq 2 \quad \text{and} \quad n = 1, \tag{7b}$$
$$= \bar{J}^{n-1}_{\theta_m}\left(\bar{r}'_c\right) \quad m \geq 1 \quad \text{and} \quad n \geq 2, \tag{7c}$$
$$= 2\hat{n} \times \bar{H}\left(\bar{r}'_c\right) \quad \begin{cases} m = 1 \ \text{and} \ n = 1 \\ m \geq 2 \ \text{and} \ n = N(m-1) + \alpha \end{cases}. \tag{7d}$$

Note that an iterative method has different convergence speeds depending on how close the initial value is to the true solution. When using this initial guess, CR(n) decreases to a value less than the threshold value within fewer iterations than required in the AIPO-CR method, because IPO-RPS makes use of better initial current estimate than do IPO and AIPO-CR.

For this new initial guess to be valid, the surfaces of the structure analyzed must change smoothly. However, the IPO-RPS method can also be applied to structures in which the surfaces change abruptly. In that case, IPO-RPS may not converge to the solution within the predetermined maximum number of iterations $N(m-1) + \alpha$. Therefore, IPO-RPS method rejects the new initial guess (Eq. (7b)), reinitializes the iterations using the traditional PO current (Eq. (7d)) as the initial value.

3. SIMULATION MODELS AND RESULTS

3.1. Models

In an open-ended cavity (Fig. 2), $\hat{n}$ is the outward unit normal vector of the aperture, $\hat{k}$ the unit wave vector, and θ the incident angle.

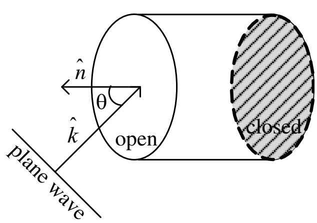

Figure 2. Open-ended cavity.

RCSs at a frequency of 10 GHz were calculated for cylindrical and rectangular cavities. The cylindrical cavities had diameter 4λ, where λ is the wavelength of the incident field, and rectangular cavities had cross-section $4\lambda \times 4\lambda$. For both cavities, the short length was 4λ and the long length was 10λ. To apply the IPO method, the aperture size of a cavity must be electrically large [19]; the cavities in this simulation satisfied this condition. The surface of the rectangular cavity had four sharp edges and was chosen to verify that the IPO-RPS method can overcome the basic assumption of smooth-surface geometry. In this simulation, $CR' = 3\%$ and $\alpha = 2$ because $N(m)$ does not increase drastically but increases gradually for each θ_m.

3.2. Results

Monostatic RCSs were obtained using IPO-RPS for all structures and were compared with results obtained using IPO, AIPO-CR, and

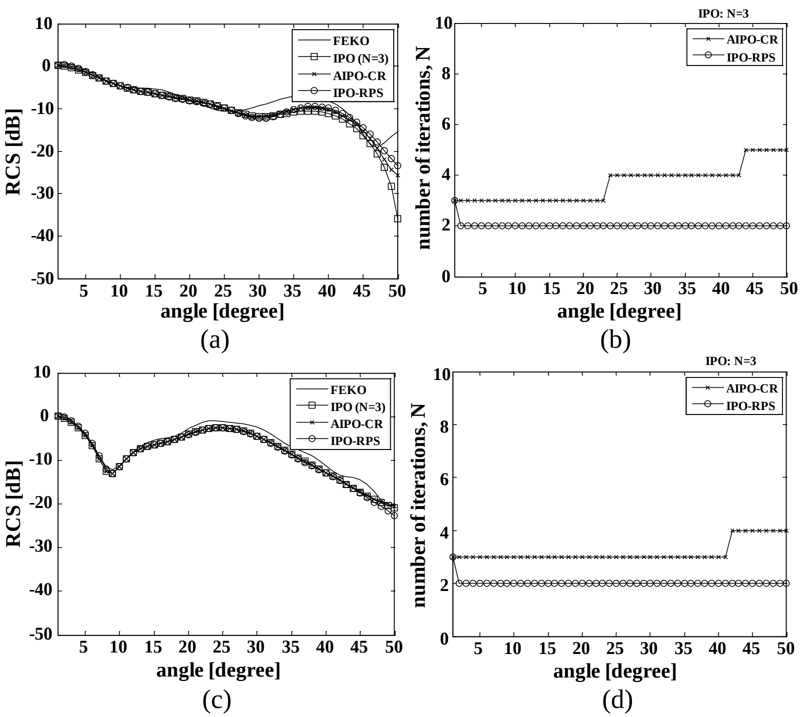

Figure 3. Results for the short cylindrical cavity. (a) Monostatic RCS patterns ($\hat{\phi}$ polarization). (b) $N(m)$ ($\hat{\phi}$ polarization). (c) Monostatic RCS patterns ($\hat{\theta}$ polarization). (d) $N(m)$ ($\hat{\theta}$ polarization).

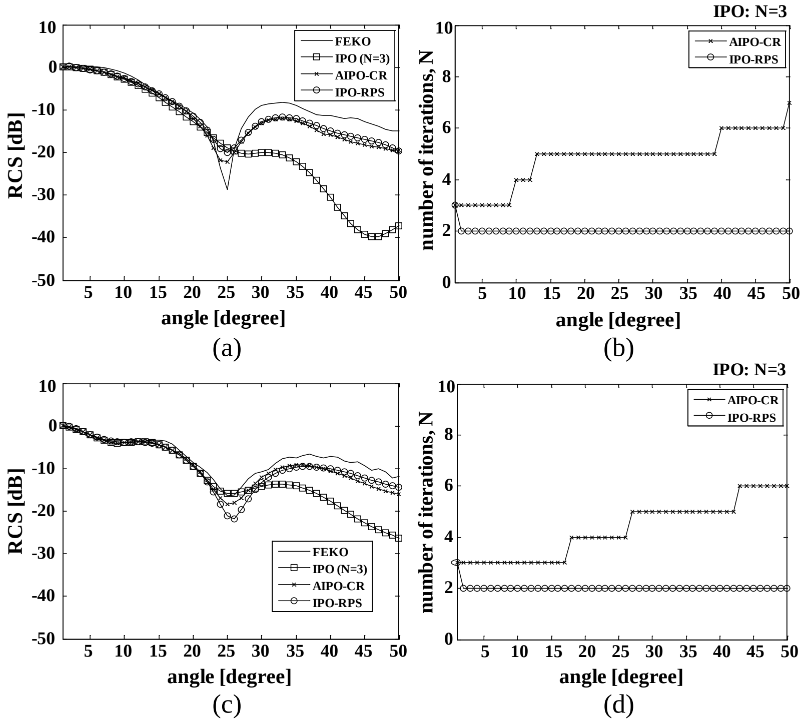

Figure 4. Results for the long cylindrical cavity. (a) Monostatic RCS patterns ($\hat{\phi}$ polarization). (b) $N(m)$ ($\hat{\phi}$ polarization). (c) Monostatic RCS patterns ($\hat{\theta}$ polarization). (d) $N(m)$ ($\hat{\theta}$ polarization).

FEKO [25] (Figs. 3–6). The total scattering fields $\bar{E}^s$ were obtained as the sum of the fields scattered by the inner cavity wall $\bar{E}_i^s$ and by the outer cavity wall $\bar{E}_o^s$. The scattering fields calculated by IPO type (IPO and its variants AIPO-CR and IPO-RPS) involved only $\bar{E}_i^s$, whereas the scattering fields calculated by FEKO involved both $\bar{E}_i^s$ and $\bar{E}_o^s$, so results obtained using methods based on IPO ($\mathrm{RCS}_{\mathrm{IPO\ type}}$) and FEKO ($\mathrm{RCS}_{\mathrm{FEKO}}$) were represented by:

$$\bar{E}^s = \bar{E}_i^s + \bar{E}_o^s, \tag{8}$$

$$\mathrm{RCS} = \lim_{r\to\infty} 4\pi r^2 \begin{cases} \left|\bar{E}_i^s(\bar{r})/\bar{E}^i(\bar{r})\right|^2 & \text{IPO type} \\ \left|\bar{E}^s(\bar{r})/\bar{E}^i(\bar{r})\right|^2 & \text{FEKO} \end{cases}, \tag{9}$$

where $\bar{E}^i$ is the incident electric field.

$\hat{\phi}$ polarization and $\hat{\theta}$ polarization stand for each direction of electric field in a spherical coordinate system, and co-polarization was assumed in this paper. The results for the short cylindrical cavity (Fig. 3) differ from those for the long cylindrical cavity (Fig. 4). For the long cylindrical cavity, N is insufficient, so the accuracy of IPO degrades as θ increases. Increasing the N of IPO yields a more accurate result but causes unnecessary time waste for incident angles at which the number of multiple reflections inside the cavity is relatively small. This problem can be circumvented by AIPO-CR using variable N, but it takes much computation time due to its poor initial guess of current, i.e., PO current. Compared to AIPO-CR, IPO-RPS with new initial guess converges to solution within much smaller N, but has similar accuracy due to the use of same convergence check criterion in Eq. (5) (Figs. 3, 4). The reduction in the maximum number of required iterations proposed IPO-RPS compared to AIPO-CR becomes

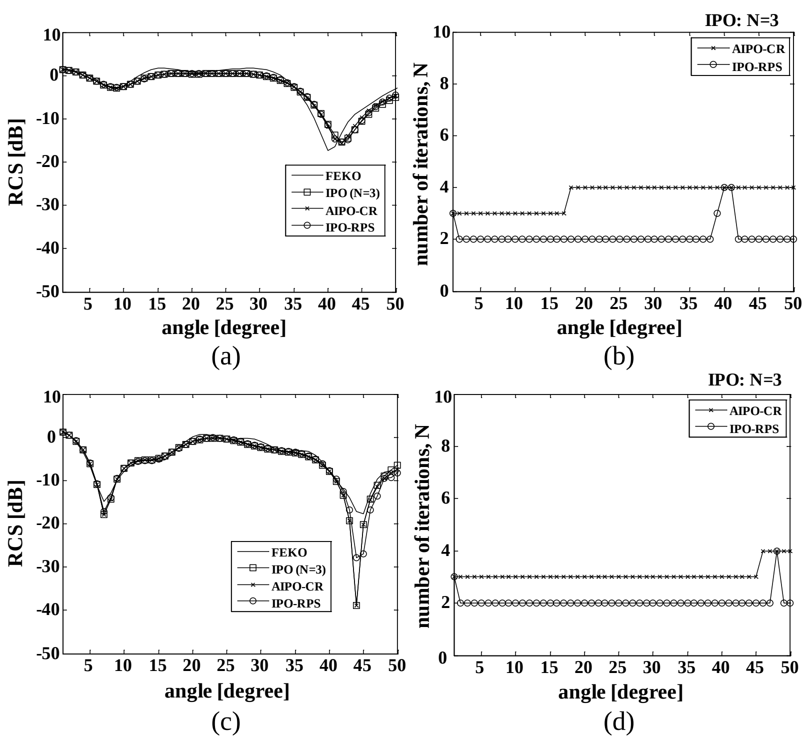

Figure 5. Results for the short rectangular cavity. (a) Monostatic RCS patterns ($\hat{\phi}$ polarization). (b) $N(m)$ ($\hat{\phi}$ polarization). (c) Monostatic RCS patterns ($\hat{\theta}$ polarization). (d) $N(m)$ ($\hat{\theta}$ polarization).

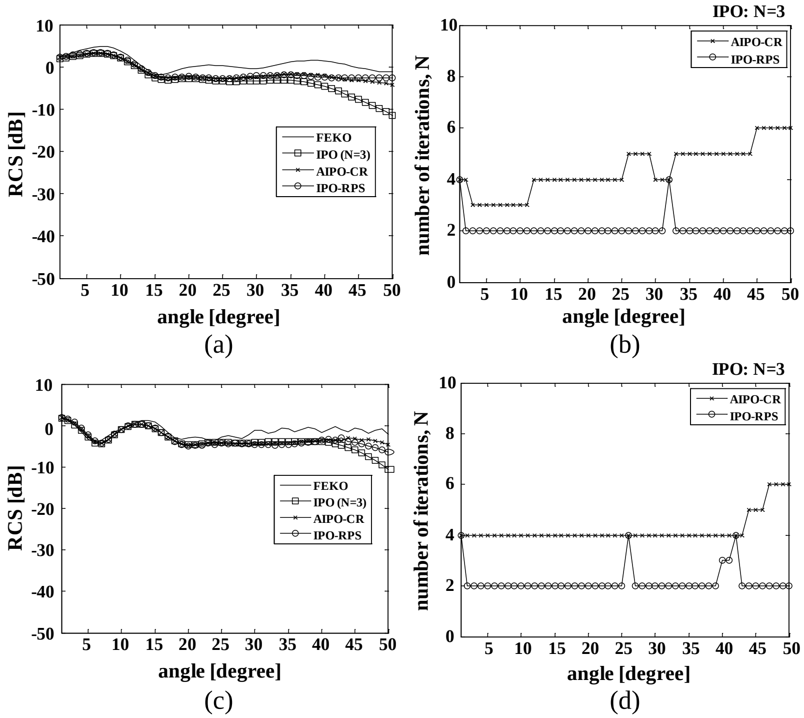

Figure 6. Results for the long rectangular cavity. (a) Monostatic RCS patterns ($\hat{\phi}$ polarization). (b) $N(m)$ ($\hat{\phi}$ polarization). (c) Monostatic RCS patterns ($\hat{\theta}$ polarization). (d) $N(m)$ ($\hat{\theta}$ polarization).

more obvious as the cavity length increases. $N(1)$ for the first incident angle θ_1 of both AIPO-CR and IPO-RPS was the same due to the use of same initial value (PO current, Eq. (7d)) to find the solution. The FEKO results become slightly different from other results as the incident angle increases because the effect of the outer cavity wall dominates at large θ.

Results for the short (Fig. 5) and long (Fig. 6) rectangular cavities show trends similar to those observe in short (Fig. 3) and long (Fig. 4) cylindrical cavities. In Figs. 5 and 6, $N(m)$ for IPO-RPS is the same as that of AIPO-CR at certain θ values. At these angles, the solution of IPO-RPS does not converge due to use of a poor initial value, so IPO-RPS was reinitialized and then applied PO current in Eq. (7d) to the initial solution of Eq. (7a). In this way, IPO-RPS is applicable not only to smooth objects but also to objects with sharp edges like rectangular cavities. Compared to AIPO-CR, IPO-RPS has comparable accuracy

Table 1. Resources to analyze the cavities using each method (Specification of the computer: Intel®Core$^{\mathrm{TM}}$2 Quad CPU Q9550 @ 2.83 GHz, 8 GB of RAM).

Cavity	Method	Number of unknowns	Memory (MB)	Computation Time (sec)	
				$\hat{\phi}$-pol.	$\hat{\theta}$-pol.
Short Cylindrical	IPO	1284	2	362	362
	AIPO-CR			436	384
	IPO-RPS			265	265
Long Cylindrical	IPO	3914	2.6	3681	3696
	AIPO-CR			5783	5190
	IPO-RPS			2608	2608
Short Rectangular	IPO	2526	2.3	1395	1395
	AIPO-CR			1673	1447
	IPO-RPS			1101	1076
Long Rectangular	IPO	5158	2.8	6486	6468
	AIPO-CR			9293	8970
	IPO-RPS			4889	5255

but requires fewer iterations (Figs. 3–6). Table 1 shows the resources request according to the methods and polarization of incident field in this simulation.

4. CONCLUSIONS

In this paper, a new approach for analyzing open-ended cavities, called IPO-RPS, has been proposed to address the drawbacks of both the traditional IPO and AIPO-CR methods. The IPO method operates with a fixed number of maximum iterations N. Therefore, for small N, its RCS prediction accuracy degrades at low computational cost, whereas for large N, its accuracy increases at high computational cost. The AIPO-CR method can improve the accuracy of the IPO solution by adaptively adjusting N for each incident angle θ_m, but requires more computation time than IPO. The proposed IPO-RPS method exploits the final current obtained at θ_{m-1} as the initial current for θ_m ($m \geq 2$). Simulation results show that compared to AIPO-CR, IPO-RPS is much faster, while maintaining comparable RCS prediction accuracy. In addition, the IPO-RPS method can be applied not only to smooth objects, but also to objects with sharp discontinuities. This results from the fact that the IPO-RPS method has a special mechanism to adaptively change its initial current between the final solution at previous incident angle θ_{m-1} and traditional PO current. The efficiency of IPO-RPS method becomes more pronounced for longer cavities having a large number of internal reflections.

ACKNOWLEDGMENT

This work was supported by the Brain Korea 21 Project in 2012.

REFERENCES

1. Harrington, R. F., *Field Computation by Moment Methods*, Macmillan, 1968.
2. Liu, Z.-L. and J. Yang, "Analysis of electromagnetic scattering with higher-order moment method and nurbs model," *Progress In Electromagnetics Research*, Vol. 96, 83–100, 2009.
3. Jin, J. M., *The Finite Element Method in Electromagnetics*, Wiley, 2002.
4. Zhang, H.-W., X.-W. Zhao, Y. Zhang, D. Garcia-Donoro, W.-X. Zhao, and C.-H. Liang, "Analysis of a large scale narrow-wall slotted waveguide array by parallel mom out-of-core solver using the higher order basis functions," *Journal of Electromagnetic Waves and Applications*, Vol. 24, Nos. 14–15, 1953–1965, 2010.
5. Taflove, A. and S. C. Hagness, *Computational Electrodynamics: The Finite-difference Time-domain Method*, Artech House, 2000.
6. Chen, C.-Y., Q. Wu, X.-J. Bi, Y.-M. Wu, and L. W. Li, "Characteristic analysis for fdtd based on frequency response," *Journal of Electromagnetic Waves and Applications*, Vol. 24, Nos. 2–3, 283–292, 2010.
7. Sirenko, K., V. Pazynin, Y. K. Sirenko, and H. Bagci, "An FFT-accelerated FDTD scheme with exact absorbing conditions for characterizing axially symmetric resonant structures," *Progress In Electromagnetics Research*, Vol. 111, 331–364, 2011.
8. Kline, M. and I. Kay, *Electromagnetic Theory and Geometrical Optics*, Wiley Interscience, New York, 1965.
9. Zhang, Z. and W.-B. Dou, "Analysis of THz imaging system with a refractive small lens array by a hybrid numerical method," *Journal of Electromagnetic Waves and Applications*, Vol. 25, Nos. 8–9, 1317–1328, 2011.
10. Balanis, C. A., *Advanced Engineering Electromagnetics*, Wiley, New York, 1989.

11. Klement, D., J. Preissner, and V. Stein, "Special problems in applying the physical optics method for backscatter computations of complicated objects," *IEEE Transactions on Antennas and Propagation,* Vol. 36, No. 2, 228–237, Feb. 1988.
12. Ma, J., S.-X. Gong, J. Ling, Y.-X. Xu, and W. Jiang, "Radiation analysis of antenna around electrically large platform using Improved MoM-PO hybrid method," *Journal of Electromagnetic Waves and Applications*, Vol. 25, No. 4, 577–587, 2011.
13. Michaeli, A., "Equivalent edge currents for arbitrary aspects of observation," *IEEE Transactions on Antennas and Propagation*, Vol. 32, No. 3, 252–258, Mar. 1984.
14. Zhang, T.-L., L. Chen, Z.-H. Yan, and B. Li, "Design of dual offset shaped reflector antenna based on DEGL algorithm," *Journal of Electromagnetic Waves and Applications*, Vol. 25, Nos. 5–6, 723–732, 2011.
15. Gibson, W. C., *The Method of Moments in Electromagnetics*, Chapman & Hall/CRC, 2007.
16. Ling, H., R.-C. Chou, and S.-W. Lee, "Shooting and bouncing rays: Calculating the RCS of an arbitrarily shaped cavity," *IEEE Transactions on Antennas and Propagation*, Vol. 37, No. 2, 194–205, Feb. 1989.
17. Gao, P. C., Y. B. Tao, and H. Lin, "Fast RCS prediction using multiresolution shooting and bouncing ray method on the GPU," *Progress In Electromagnetics Research*, Vol. 107, 187–202, 2010.
18. Lim, H., J.-H. Park, J.-H. Yoo, C. H. Kim, K. Kwon, and N. H. Myung, "Joint time-frequency analysis of RADAR micro-doppler signatures from aircraft engine models," *Journal of Electromagnetic Waves and Applications*, Vol. 25, Nos. 8–9, 1069–1080, 2011.
19. Obelleiro-Basteiro, F., J. L. Rodriguez, and R. J. Burkholder, "An iterative physical optics approach for analyzing the electromagnetic scattering by large open-ended cavities," *IEEE Transactions on Antennas and Propagation,* Vol. 43, No. 4, 356–361, Apr. 1995.
20. Hemon, R., P. Pouliguen, H. He, J. Saillard, and J.-F. Damiens, "Computation of EM field scattered by an open-ended cavity and by a cavity under radome using the iterative physical optics," *Progress In Electromagnetics Research*, Vol. 80, 77–105, 2008.
21. Li, J., B. Wei, Q. He, L.-X. Guo, and D.-B. Ge, "Time-domain iterative physical optics method for analysis of EM scattering from the target half buried in rough surface: PEC case," *Progress In Electromagnetics Research*, Vol. 121, 391–408, 2011.

22. Choi, S. H., D. W. Soe, and N. H. Myung, "Scattering analysis of open-ended cavity with inner object," *Journal of Electromagnetic Waves and Applications*, Vol. 21, No. 12, 1689–1702, 2007.
23. Lim, H. and N.-H. Myung, "A novel hybrid AIPO-MoM technique for jet engine modulation analysis," *Progress In Electromagnetics Research*, Vol. 104, 85–97, 2010.
24. Chew, W. C., J. M. Jin, E. Michielssen, and J. M. Song, *Fast and Efficient Algorithm in Computational Electromagnetics*, Artech House, 2001.
25. FEKO, EM Software & Systems, S.A. (Pty) Ltd., www.feko.info.